Featured in Physics

# First Measurement of Neutrino Emissions from Spent Nuclear Fuel by the Double Chooz Experiment

T. Abrahão,[1,2] H. Almazan,[3,c] J. C. dos Anjos,[1] S. Appel,[4] J. C. Barriere,[5] I. Bekman,[6] T. J. C. Bezerra,[7,d] L. Bezrukov, E. Blucher,[8] C. Bourgeois,[9] C. Buck,[3] J. Busenitz,[10] A. Cabrera,[2,9,11] M. Cerrada,[12] E. Chauveau,[13] P. Chimenti,[1,e] O. Corpace,[5] J. V. Dawson,[2] J. F. Du,[9,11] Z. Djurcic,[14] A. Etenko, H. Furuta,[15] I. Gil-Botella,[12] A. Givaudan,[2] H. Gomez,[2,5] M. C. Goodman,[14] T. Hara,[16] J. Haser,[3] D. Hellwig,[6] A. Hourlier,[2] M. Ishitsuka,[17,f] J. Jochum,[18] C. Jollet,[13] K. Kale,[13] M. Kaneda,[17] M. Karakac,[2] T. Kawasaki,[19] E. Kemp,[20] D. Kryn,[2] M. Kuze,[17] T. Lachenmaier,[18] C. E. Lane,[21] T. Lasserre,[2,5,3,a] D. Lhuillier,[5] H. P. Lima, Jr.,[1,g] M. Lindner,[3] J. M. LoSecco,[22] B. Lubsandorzhiev, J. Maeda,[23,16] C. Mariani,[24] J. Maricic,[21,h] J. Martino,[7] T. Matsubara,[23,i] G. Mention,[5] A. Meregaglia,[13] T. Miletic,[21,j] R. Milincic,[21] A. Minotti,[5] X. Mougeot,[25] D. Navas-Nicolás,[12,9] Y. Nikitenko,[6] P. Novella,[12,k] L. Oberauer,[4] M. Obolensky,[2] A. Onillon,[5,3,b] A. Oralbaev,[2] C. Palomares,[12] I. M. Pepe,[1] L. Perisse,[5,l] G. Pronost,[7,m] J. Reichenbacher,[10,n] S. Schönert,[4] S. Schoppmann,[3,o] L. Scola,[5] R. Sharankova,[17] V. Sibille,[5] V. Sinev, M. Skorokhvatov, P. Soldin,[6] A. Stahl,[6] I. Stancu,[10] M. R. Stock,[4] L. F. F. Stokes,[18] F. Suekane,[15] S. Sukhotin, T. Sumiyoshi,[23] C. Veyssiere,[5] B. Viaud,[7] M. Vivier,[5] S. Wagner,[2] C. Wiebusch,[6] G. Yang,[14,p] and F. Yermia[7]

(Double Chooz Collaboration)

[1]*Centro Brasileiro de Pesquisas Físicas, Rio de Janeiro, RJ, 22290-180, Brazil*
[2]*APC, Université de Paris, CNRS, Astroparticule et Cosmologie, F-75006, Paris*
[3]*Max-Planck-Institut für Kernphysik, 69117 Heidelberg, Germany*
[4]*Physik Department, Technische Universität München, 85748 Garching, Germany*
[5]*IRFU, CEA, Université Paris-Saclay, 91191 Gif-sur-Yvette, France*
[6]*III. Physikalisches Institut, RWTH Aachen University, 52056 Aachen, Germany*
[7]*Subatech, CNRS, Université de Nantes, IMT-Atlantique, 44307 Nantes, France*
[8]*The Enrico Fermi Institute, The University of Chicago, Chicago, Illinois 60637, USA*
[9]*IJC Laboratory, CNRS, Université Paris-Saclay, Orsay, France*
[10]*Department of Physics and Astronomy, University of Alabama, Tuscaloosa, Alabama 35487, USA*
[11]*LNCA Underground Laboratory, CNRS-CEA, Chooz, France*
[12]*Centro de Investigaciones Energéticas, Medioambientales y Tecnológicas, CIEMAT 28040, Madrid, Spain*
[13]*Université de Bordeaux, CNRS, LP2I, UMR 5797, F-33170 Gradignan, France*
[14]*Argonne National Laboratory, Argonne, Illinois 60439, USA*
[15]*Research Center for Neutrino Science, Tohoku University, Sendai 980-8578, Japan*
[16]*Department of Physics, Kobe University, Kobe 657-8501, Japan*
[17]*Department of Physics, Institute of Science Tokyo, Tokyo 152-8551, Japan*
[18]*Kepler Center for Astro and Particle Physics, Universität Tübingen, 72076 Tübingen, Germany*
[19]*Department of Physics, Kitasato University, Sagamihara 252-0373, Japan*
[20]*Universidade Estadual de Campinas-UNICAMP, Campinas, SP, 13083-970, Brazil*
[21]*Department of Physics, Drexel University, Philadelphia, Pennsylvania 19104, USA*
[22]*University of Notre Dame, Notre Dame, Indiana 46556, USA*
[23]*Department of Physics, Tokyo Metropolitan University, Tokyo 192-0397, Japan*
[24]*Center for Neutrino Physics, Virginia Tech, Blacksburg, Virginia 24061, USA*
[25]*Université Paris-Saclay, CEA, List, Laboratoire National Henri Becquerel (LNE-LNHB), F-91120, Palaiseau, France*

[a]Contact author: thierry.lasserre@mpi-hd.mpg.de
[b]Contact author: anthony.onillon@mpi-hd.mpg.de
[c]Present address: Donostia International Physics Center (DIPC), BERC Basque Excellence Research Centre, Donostia, Spain.
[d]Present address: Department of Physics and Astronomy, University of Sussex, Falmer, Brighton, United Kingdom.
[e]Present address: Universidade Estadual de Londrina, 86057-970 Londrina, Brazil.
[f]Present address: Tokyo University of Science, Noda, Chiba, Japan.
[g]Present address: Gran Sasso Science Institute, 67100 L'Aquila, Italy.
[h]Present address: Physics and Astronomy Department, University of Hawaii at Manoa, Honolulu, Hawaii, USA.
[i]Present address: High Energy Accelerator Research Organization (KEK), Tsukuba, Ibaraki, Japan.
[j]Present address: Physics Department, Arcadia University, Glenside, Pennsylvania 19038, USA.

(Received 6 October 2025; revised 22 April 2026; accepted 1 June 2026; published 4 August 2026)

Neutrino emission from nuclear reactors provides real-time insights into reactor power and fuel evolution, with potential applications in monitoring and nuclear safeguards. Following reactor shutdown, a low-intensity flux of "residual neutrinos" persists due to the decay of long-lived fission isotopes in the partially burnt fuel remaining within the reactor cores and in spent nuclear fuel stored in nearby cooling pools. The Double Chooz experiment at the Chooz B nuclear power plant in France achieved the first quantitative measurement of this residual flux based on 17.2 days of reactor-off data. In the energy range where the residual signal is most pronounced, the neutrino detector located 400 m from the cores recorded $106 \pm 18$ neutrino candidate events ($5.9\sigma$ significance). This measurement is in excellent agreement with the predicted value of $88 \pm 7$ events derived from detailed reactor simulations modeling the decay activities of fission products and incorporating the best-available models of neutrino spectra.

DOI: 10.1103/dr26-j19g

Nuclear reactor cores are the largest source of man-made electron antineutrinos ($\bar{\nu}_e$), produced via the $\beta$ decay of neutron-rich fragments generated primarily during the fission of heavy elements such as uranium and plutonium. Physicists have detected $\bar{\nu}_e$ from reactors for more than six decades [1]. The emitted $\bar{\nu}_e$'s have unique inherent features that make them of particular interest to International Atomic Energy Agency (IAEA) safeguards, as they are nonalterable and inextricably linked to the nuclear processes occurring in the reactor core [2]. This concept, pioneered by Borovoi and Mikaelyan in 1978 [3], was first implemented at the ROVNO power station in 1985 [4]. Neutrino emission provides real-time, nonintrusive information about the operational state and fissile content of a reactor core. At leading order, the neutrino flux scales with the total number of fissions, while at the next order, it is influenced by the specific isotopic composition undergoing fission. Neutrino detectors can therefore be used to detect anomalies in neutrino emissions from the cores, indicating possible diversion of nuclear material. Usually, the inverse $\beta$-decay (IBD) capture reaction, $\bar{\nu}_e + p \to e^+ + n$, is used for detection. Beyond the monitoring of operating nuclear units, several other promising applications of neutrino-based safeguards have been identified through a collaboration between the IAEA and neutrino physics experts [2]. Among these, the verification of the spent fuel inventory and the estimation of the residual power of the reactor when the core is shut down or following a potential nuclear incident are two topics frequently discussed but not yet quantitatively studied using neutrino data collected during a reactor-off period [5,6].

After reactor shutdown, a residual neutrino flux continues to be emitted from the decay of long-lived fission products (FPs) present in burnt fuel assemblies still in the reactor core, as well as those previously removed from the cores and stored in nearby spent fuel cooling pools. This residual flux, typically accounting for less than 1% of the nominal reactor signal, is theoretically well understood but has never been measured. Its detection requires low background conditions, a well-understood detector response, and controlled systematics. In this Letter, we present the first quantitative measurement of this residual neutrino flux and its energy spectrum, obtained with the Double Chooz neutrino experiment [7], located in the French Ardennes near the two 4.25 $GW_{th}$ cores of the Chooz B nuclear power plant and originally operated to study neutrino oscillations [8].

*Post-fission* $\bar{\nu}_e$—The Chooz reactor cores are pressurized water reactors (PWRs), each containing 205 fuel assemblies composed of approximately 600 kg of enriched uranium dioxide ($UO_2$), primarily $^{238}$U with a few percent of $^{235}$U. During operation, additional fissile isotopes, $^{239}$Pu and $^{241}$Pu, are produced through neutron capture and subsequent decay processes involving $^{238}$U. The fission of these four isotopes ($^{235}$U, $^{238}$U, $^{239}$Pu, $^{241}$Pu) accounts for more than 99.7% of the core's thermal power. The reactors typically operate at full power for over a year in what is known as an irradiation cycle, followed by a refueling

[k]Present address: Instituto de Física Corpuscular, IFIC (CSIC and UV), 46980 Paterna, Spain.
[l]Present address: ILANCE, CNRS—University of Tokyo International Research Laboratory, Kashiwa, Chiba 277-8582, Japan.
[m]Present address: Kamioka Observatory, ICRR, University of Tokyo, Kamioka, Gifu 506-1205, Japan.
[n]Present address: South Dakota School of Mines and Technology, Rapid City, South Dakota 57701, USA.
[o]Present address: Johannes Gutenberg-Universität Mainz, Detektorlabor, Exzellenzcluster PRISMA+, Mainz, Germany.
[p]Present address: State University of New York at Stony Brook, Stony Brook, New York 11755, USA.

period during which the reactor is shut down for 6–8 weeks. During this period, about one third of the spent fuel assemblies are removed and transferred to storage pools located in an adjacent building, approximately 38 m from the reactor cores. Each assembly typically undergoes three irradiation cycles and reaches a burnup of approximately 45 GW·days/ton before being removed. For $UO_2$ fuel with 4% enrichment, this burnup typically corresponds to the consumption of ~75%–80% of the initial fissile material. The spent fuel assemblies are then cooled in storage pools for several years before being transported off site for reprocessing. Electron antineutrinos ($\bar{\nu}_e$) are mainly produced by the $\beta^-$ decay of FPs and, to a lesser extent, by neutron capture reactions forming isotopes such as $^{239}$U and $^{239}$Np. However, only $\bar{\nu}_e$ from FPs are detectable due to the 1.8 MeV threshold of the IBD reaction. Most fission-induced $\bar{\nu}_e$ are emitted promptly following fission events. During reactor operation, long-lived FPs gradually accumulate in the fuel. After shutdown, these isotopes continue to decay, producing a small residual $\bar{\nu}_e$ flux that decreases over time. Around a reactor, the intensity and spectral shape of this residual flux depend on both the irradiation history and the time elapsed since shutdown, with contributions from fuel assemblies still in the cores and in nearby cooling pools.

*The Double Chooz experiment*—A two-detector setup was used to measure the $\theta_{13}$ neutrino mixing angle, with detectors placed at average distances of 400 m and 1.05 km from the reactor cores to observe neutrino oscillations [7]. The experiment operated from 2011 to 2017, with the far detector (FD) starting in 2011 and the near detector (ND) joining in 2014 to complete the two-detector setup. Both detectors, shielded underground by 115 (ND) and 300 m (FD) water equivalent, were identically designed to minimize systematic uncertainties and enable precise near and far comparisons of $\bar{\nu}_e$ rates and energy spectra [9]. The experimental layout, showing detector positions relative to the reactor cores and spent fuel pools, is illustrated in Fig. 1. Unlike multicore reactor experiments such as Daya Bay [10] and RENO [11], where simultaneous core shutdowns never occurred, the two-core configuration of the Chooz B plant enabled *in situ* background measurements during such events. This unique feature not only strengthened the original oscillation analysis [7,12] but also provides a rare opportunity to measure residual $\bar{\nu}_e$ emission. Each detector consisted of four concentric volumes topped by an outer muon veto system. The innermost volume (*neutrino target*, NT) was filled with 10.3 m$^3$ of Gd-loaded (1 g/l) liquid scintillator, surrounded by a 22.6 m$^3$ *gamma catcher* (GC) filled with unloaded scintillator to ensure full calorimetry of interactions associated with neutron capture on Gd. These two volumes, along with the 105 cm-thick buffer tank filled with non-scintillating mineral oil and instrumented with 390 low-background 10-inch photomultiplier tubes (PMTs), formed the *inner detector* (ID). The ID was

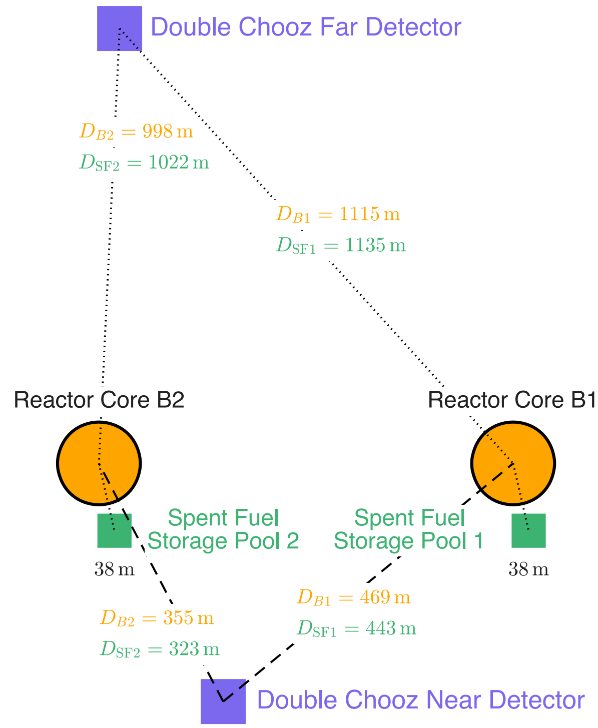


FIG. 1. Schematic of the Double Chooz layout, showing the far and near detectors relative to reactor cores (B1, B2) and their spent fuel pools.

surrounded by a 50 cm-thick liquid scintillator *inner muon veto* (IV) equipped with 78 8-inch PMTs. The far detector was shielded from rock radiation by 15 cm of demagnetized steel, while the near detector was shielded by 1 m of water. An *outer muon veto* (OV), consisting of segmented scintillator modules positioned above the detector, provided additional rejection of cosmic muons. Reactor $\bar{\nu}_e$ were detected via the IBD process, primarily occurring in the NT and GC. At full reactor power, the near and far detectors recorded about 900 and 140 IBD events/day, respectively [7].

*Dataset*—Between 2011 and 2017, the Double Chooz experiment recorded rare reactor-off periods when both reactor cores were simultaneously offline. This scenario was uncommon due to the plant's alternating refueling schedules. A first analysis of such conditions, based on 7.5 days of reactor-off data collected in 2011–2012 with only the far detector, validated the predicted background model for the oscillation analysis [13]. However, the limited duration of that period and the absence of near-detector data resulted in only ~20 IBD candidates, preventing any extraction of a residual reactor $\bar{\nu}_e$ spectrum. In the present Letter, we exploit a much larger dataset collected in 2017, during four reactor-off intervals in which both cores were simultaneously shut down for refueling or maintenance. As shown in Fig. 2, these intervals totaled 24.4 days (1.6, 1.1, 1.0, and 20.8 days), providing the statistics needed for a quantitative residual-flux

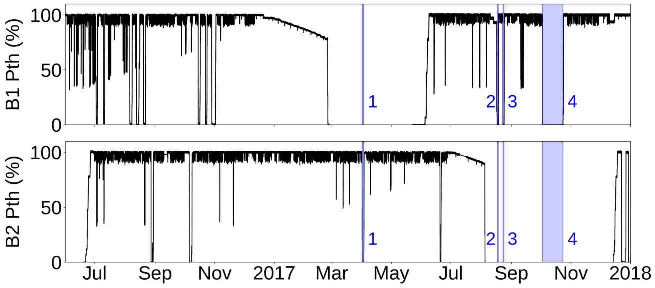


FIG. 2. Thermal power history of reactor cores B1 and B2, with the four reactor-off periods in 2017 highlighted in blue.

TABLE I. Background-subtracted and expected residual $\bar{\nu}_e$ rates for the near and far detectors.

| Rate (day$^{-1}$) | ND (400 m) | FD (1.05 km) |
|---|---|---|
| *Data—Background* | | |
| [1, 3] MeV | $6.2 \pm 1.1$ | $1.2 \pm 0.6$ |
| [3, 9] MeV | $-2.3 \pm 1.5$ | $-0.4 \pm 0.4$ |
| *Expected residual* $\bar{\nu}_e$ | | |
| [1, 3] MeV | $5.1 \pm 0.4$ | $0.7 \pm 0.1$ |
| [3, 9] MeV | $0.1 \pm 0.1$ | $0.1 \pm 0.1$ |

measurement. After accounting for muon veto–induced dead time, the detector live time amounted to 17.2 days for the near detector and 22.2 days for the far detector.

The analysis was performed for both near and far detectors; however, we focus primarily on the near detector in the following due to its closer proximity to the reactor cores and spent fuel pools, offering higher sensitivity to this low-rate signal.

*Data analysis*—The IBD detection relies on the characteristic time and spatial correlation between a prompt signal, produced by the positron's ionization ($e^+$) and annihilation, and a delayed signal from neutron (n) capture. The positron's energy deposition directly correlates with the reactor $\bar{\nu}_e$ energy, with $E_{\bar{\nu}_e} \simeq E_{e^+} + 0.78$ MeV. IBD event selection follows the same criteria as the oscillation analysis in [7], employing the total neutron capture (TnC) method, which, in addition to gadolinium, includes neutron captures on carbon and hydrogen across all ID volumes. After applying vetoes based on the ID, IV and OV to reduce muon-induced backgrounds, IBD candidates are selected within a 0.5–800 μs time window and a spatial separation of 0–1.2 m between the prompt and delayed signals. The energy windows for the prompt and delayed signals are set to [1, 20] MeV and [1.3, 10] MeV, respectively. A high-efficiency artificial neural network (ANN) was used to further suppress accidental background contamination by analyzing the time, spatial, and energy correlations of the delayed signals. As detailed in Refs. [7,14], the classifier is a multilayer-perceptron with one hidden layer of nine nodes, trained on off-time accidental pairs from data and IBD Monte Carlo events. It is applied after the loose IBD preselection and used as a multivariate classifier on this sample, with the final selection defined by a cut on its discriminant output. Two types of backgrounds mimic the $\bar{\nu}_e$ signal: correlated and accidental. Due to the relatively shallow detector overburden, correlated backgrounds are dominated by muon-induced processes. These arise primarily from fast neutrons generated by muon interactions in the surrounding rock and from $\beta$-n decays of isotopes such as $^9$Li, produced by muon spallation on $^{12}$C. The rate of $\beta$-n emitters is reduced by tagging their temporal and spatial correlations with the parent muon. FN rates and energy spectra are estimated using energy depositions tagged by the IV and OV systems up to 20 MeV. Contributions from other sources, such as stopping muons, $\beta$-n decays of $^8$He, and $\beta^-$ decay of $^{12}$B, are found to be negligible. Accidental backgrounds, caused by random coincidences of natural radioactivity and neutron captures, are strongly suppressed by the ANN, with a rejection power exceeding 400. The residual accidental rate is measured *in situ* using off-time windows within the ID, following Refs. [7,14]. These selections, applied in the 1–9 MeV energy range, yield 517 IBD candidates in the near detector, corresponding to a rate of $30.0 \pm 1.4$ events/day, prior to background substraction. In the far detector, 189 IBD candidates are observed, yielding $8.5 \pm 0.7$ events/day. The estimated background rates in the same energy window are $26.2 \pm 1.4$ and $7.7 \pm 0.2$ events/day, respectively. A summary of the residual $\bar{\nu}_e$ rates, after background subtraction, is provided in Table I. Further details on the detector properties, calibration, data selection, and background estimation are provided in [7].

*Residual* $\bar{\nu}_e$ *prediction*—A detailed summation method model of the residual $\bar{\nu}_e$ rate and energy spectrum emitted from both the reactor cores and the spent fuel pools has been developed for the four reactor-off periods following an approach similar to that in [15,16]. This model relies on coupling FP activity predictions with a database of $\bar{\nu}_e$ spectra from $\beta$ decay.

The FP activities are computed using the APOLLO-2.8.4 and DARWIN-3 simulation codes [17,18], based on the JEFF-3.1.1 nuclear data library [19]. These widely used and validated tools for neutron transport and residual power calculations simulate the time evolution of the fuel's isotopic composition and activity during both irradiation phases and cooling periods.

A similar procedure was used to simulate each fuel assembly, whether located in the reactor core or stored in the spent fuel pool during shutdown periods. This involved simulating the individual irradiation history of each assembly up to the beginning of each reactor-off period, including a detailed follow-up of the thermal power it experienced throughout its lifetime as well as any cooling periods between irradiation cycles and after its removal to the spent-fuel pool. An optimized, high-resolution temporal discretization was used to accurately model the buildup and decay of both short- and long-lived fission product isotopes. Residual $\bar{\nu}_e$ spectra are obtained by coupling the predicted FP activities with the BESTIOLE library [20]. BESTIOLE models $\bar{\nu}_e$ emission by summing individual $\beta$ branches using an advanced formalism based on Fermi theory, including electromagnetic corrections, finite nuclear size, atomic screening, and shape factors for both allowed and forbidden transitions. Particular care is taken in modeling first forbidden nonunique transitions, several of which, such as $^{144}$Pr a major contributor to the residual $\bar{\nu}_e$ flux below 3 MeV, incorporate detailed nuclear structure calculations. The IBD spectrum in each detector is obtained by integrating the time-dependent flux over the duration of the reactor-off periods and summing over all sources:

$$\frac{dN_{\bar{\nu}_e}}{dE_{\mathrm{vis}}} = \sum_i \frac{N_p}{4\pi L_i^2} \iint \phi_i(E,t)\sigma_{\mathrm{IBD}}(E) \times P_{ee}(E,L_i)\mathcal{D}(E_{\mathrm{vis}}|E)\mathrm{d}E\,\mathrm{d}t, \tag{1}$$

where $i$ runs over the two reactor cores and the two spent fuel pools, $N_p$ is the number of target protons, $L_i$ is the baseline to the source $i$, $\phi_i(E,t)$ is the time-dependent energy spectrum of the emitted $\bar{\nu}_e$, $\sigma_{\mathrm{IBD}}(E)$ is the inverse $\beta$-decay cross section, $P_{ee}(E,L_i)$ is the survival probability for baseline $L_i$, and $\mathcal{D}(E_{\mathrm{vis}}|E)$ is the detector response, which folds energy scale, resolution, and selection efficiency to map the true antineutrino energy $E$ onto the reconstructed (visible) energy $E_{\mathrm{vis}}$. The IBD cross section formalism of [21], using neutron lifetime value from [22] is used. For this calculation, the oscillation parameter $\sin^2(2\theta_{13}) = 0.105 \pm 0.014$ from the latest Double Chooz analysis is used [7], yielding mean survival probabilities of $0.978 \pm 0.003$ for the near detector and $0.909 \pm 0.012$ for the far detector.

To first order, the rate and energy spectrum of residual $\bar{\nu}_e$ emitted by a burnt fuel assembly are primarily determined by the burnup achieved before shutdown, which sets the inventory of accumulated fission products. As shown in Fig. 3 for a representative $UO_2$ assembly irradiated to 45 GWd/t, the predicted IBD $\bar{\nu}_e$ spectrum exhibits a rapid decline in both intensity and mean energy following reactor shutdown. As short-lived isotopes decay, the IBD mean cross section per fission (MCSPF) decreases by 1, 2, and 3 orders of magnitude after ~10 min, ~15 h, and ~2.5 y, respectively. Over the same period, the mean $\bar{\nu}_e$ energy drops from ~4.2 MeV to ~3.2 MeV, and eventually to ~2.7 MeV. Immediately after shutdown, the flux results from the superposition of hundreds of $\beta$ branches from many fission products. Within a few hours, however, it becomes dominated by a small number of longer-lived isotopes. After several months, the primary contributors are the short-lived isotopes $^{90}$Y ($T_{1/2} = 3.19$ h, $Q_\beta = 2.28$ MeV), $^{106}$Rh (30.1 s, 3.54 MeV), and $^{144}$Pr

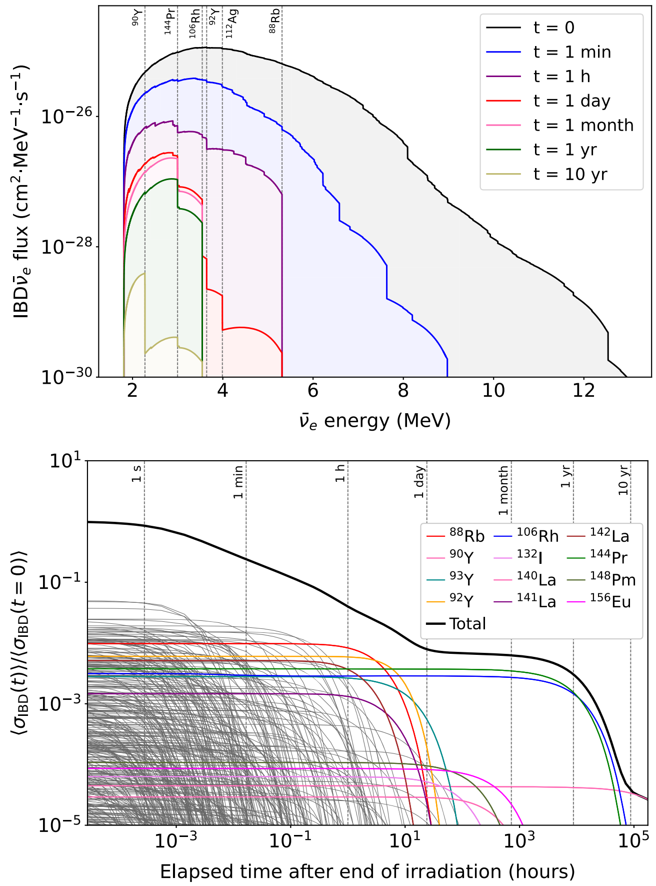


FIG. 3. Time evolution of the predicted IBD spectrum (top) and IBD MCSPF (bottom) for a representative $UO_2$ (4 wt% enrichment) spent fuel assembly irradiated to 45 GWd/t. Isotope contributions to the MCSPF are gray; dominant ones after one hour are colored.

(17.3 min, 3.00 MeV), whose long-lived precursors have accumulated in the fuel: $^{144}$Ce–$^{144}$Pr ($T_{1/2} = 285$ d), $^{106}$Ru–$^{106}$Rh (372 d), and $^{90}$Sr–$^{90}$Y (28.9 y). Beyond ten years, $^{90}$Y alone accounts for more than 90% of the residual flux.

*Reactor and pool contributions*—Burnt fuel assemblies remaining in the reactor core during refueling or maintenance are a significant source of residual $\bar{\nu}_e$ in the early stages of a reactor-off period, i.e., within the first tens of hours after shutdown, when the flux is strongly influenced by short-lived isotopes. In contrast, spent fuel stored in cooling pools contributes a long-lived component to the residual flux. Unlike burnt fuel, this contribution arises from the cumulative emission of assemblies removed over multiple fuel cycles. Some have been cooling for years, while others were removed more recently, resulting in a broad distribution of cooling times and activity levels that shapes both the intensity and spectrum of the emitted $\bar{\nu}_e$.

Figure 4 shows the predicted residual $\bar{\nu}_e$ IBD spectrum for the Double Chooz near detector, including contributions from both reactor cores and spent fuel pools. The predicted

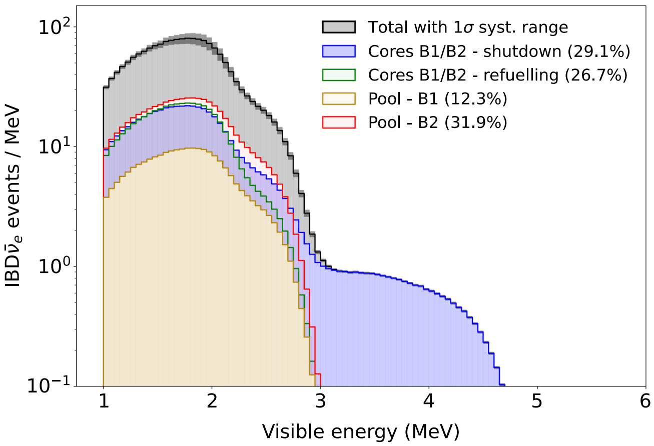


FIG. 4. Predicted IBD spectrum in the near detector for all reactor-off periods stacked and combined, showing contributions from two reactor cores, two spent fuel pools, and the total spectrum.

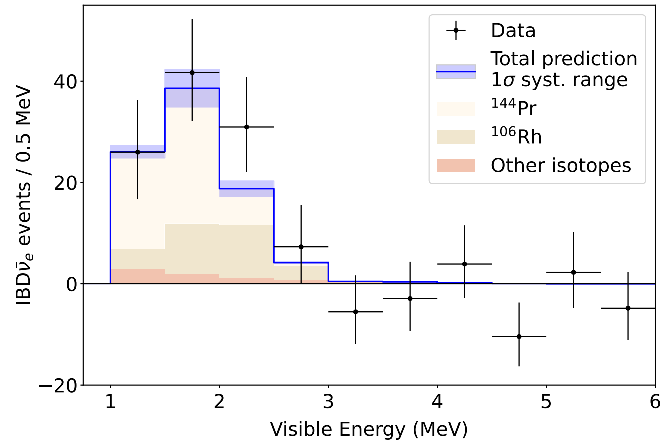


FIG. 5. Measured residual $\bar{\nu}_e$ spectrum in the Double Chooz near detector (background subtracted), compared with the prediction, highlighting contributions from the dominant isotope contributors. In the 1–3 MeV range, $106 \pm 18$ events are observed, compared to a prediction of $88 \pm 7$ events.

IBD spectrum extends up to approximately 4.5 MeV with 98.7% of the residual flux expected below 3 MeV. An energy-integrated contribution of 56% from the reactors and of 44% from the storage pools is obtained. While residual $\bar{\nu}_e$ emission is initially dominated by burnt fuel still in the reactors due to the presence of short-lived isotopes, the long-term emission from spent fuel pools, integrating multiple assemblies with varying cooling times, becomes comparable over extended reactor-off periods. The B1 pool (yellow area) contributes less than B2 (red area) because the longest reactor-off period coincided with the refueling of reactor B2. During this time, a new batch of spent fuel was added to the B2 pool (red line), increasing its relative contribution to the total residual $\bar{\nu}_e$ flux. Further details on the time evolution of the individual residual-signal components are given in the End Matter [23]. The total normalization uncertainty on the predicted residual $\bar{\nu}_e$ signal in the near detector is 7.4%, dominated by a 6.0% uncertainty in antineutrino spectrum modeling. This uncertainty arises primarily from nuclear-structure uncertainties affecting the dominant first-forbidden transitions of $^{144}$Pr. Conservatively, the $1\sigma$ uncertainty on the $^{144}$Pr spectral shape was defined as the difference between the shape factor obtained from the detailed nuclear-structure calculations and that obtained using the simplified $\xi$ approximation, which assumes an allowed transition. Other significant contributions come from geometric baseline uncertainties (2.9%), the simulated fission product inventory (2.1%), and the estimated amount of spent fuel assemblies in the pools (2.0%). The latter includes a conservative treatment of older assemblies whose status is uncertain, by assigning a 100% uncertainty to their contribution. Detector-related systematics are subdominant, contributing less than 0.8% in total.

*Results*—Measured and predicted residual $\bar{\nu}_e$ rates are summarized in Table I for different energy ranges. In the near detector, a significant excess of IBD events is observed in the 1–3 MeV window, where the residual signal is expected to peak, as clearly shown in Fig. 5. In this range, $106 \pm 18$ residual candidates are observed, in good agreement with the prediction of $88 \pm 7$ ($\Delta \equiv \text{data} - \text{prediction} = 18 \pm 19$), both in rate and in spectral shape. The measurement uncertainty is dominated by statistical fluctuations in the observed IBD candidates, with a total of 244 events recorded in the 1–3 MeV range, before background subtraction. For the combined 17.2 days of reactor-off livetime in the near detector, this corresponds to an averaged predicted residual $\bar{\nu}_e$ flux at the detector of $\Phi_{\text{res}} \simeq 3.6 \times 10^8\ \text{cm}^{-2}\,\text{s}^{-1}$ (spent-fuel pools: $1.6 \times 10^8\ \text{cm}^{-2}\,\text{s}^{-1}$, reactor cores: $2.0 \times 10^8\ \text{cm}^{-2}\,\text{s}^{-1}$) for antineutrino energies above the 1.8 MeV IBD threshold. In this energy range, the residual background is dominated by $86 \pm 8.3$ correlated events, with $52.1 \pm 0.1$ accidental events after ANN suppression. The flux in this region is expected to be dominated by $^{144}$Pr (~54%) and $^{106}$Rh (~38%), with minor isotopes accounting for the remainder. In the far detector, a smaller excess of $27 \pm 13$ events is observed in the same energy range, compared to the predicted $14 \pm 1$. Although this measurement is also in good agreement with the prediction, the larger baseline suppresses both the event rate and the statistical significance relative to the near detector. Above 3 MeV, no significant excess is observed in either detector. In this region, the background-subtracted yields are consistent with zero (see Table I), validating the background model and confirming that the small high-energy residual tail, predicted at a rate below 0.1 events/day, lies well below the current sensitivity.

*Conclusion*—Over the past two decades, the IAEA safeguards community and the neutrino-physics community have jointly explored how reactor antineutrinos could be used for nonintrusive monitoring of nuclear facilities [2]. Several reactor-on demonstrations have been performed, but the specific case of spent-fuel verification had, until now, remained untested experimentally [24].

The present Letter shows that dedicated reactor-off operation of the Double Chooz near detector delivers sufficient statistics (17.2 days) and low backgrounds to extract, for the first time, a quantitative residual reactor antineutrino spectrum. In combination with a spent-fuel simulation, this provides the first direct validation of residual-flux predictions, including contributions from both reactor cores and spent-fuel pools. In the 1–3 MeV range, where the residual neutrino signal is strongest, the observed $106 \pm 18$ events represent a $5.9\sigma$ excess over background, in very good agreement with the predicted $88 \pm 7$ events. The significance is obtained directly from event counting, using $Z = N_{\mathrm{res}}/\sigma_{\mathrm{res}}$. The measurement uncertainty is of the order of one half of the predicted spent-fuel-pool contribution to the residual signal. It therefore indicates that the present measurement is sensitive to the existence of this residual signal and to large changes in the overall inventory, but not to the diversion of a small number of assemblies.

This result establishes a robust experimental benchmark for residual-reactor and spent-fuel neutrino monitoring at baselines of a few hundred meters. From a safeguards perspective, it turns earlier conceptual studies into an experimental proof of principle: neutrinos can be used to monitor reactor conditions during shutdown and to obtain information on nearby spent fuel in a direct and nonintrusive way. On this basis, realistic performance targets can now be set for future, more portable and lower-cost detectors. The most natural use cases are compact fuel-storage configurations, such as spent-fuel pools or small dry-cask pads holding a limited number of assemblies, where neutrino-based nonintrusive and nondestructive assay would provide a quantitative, independent complement to today's largely accounting-based verification, albeit at the price of sizable detector systems and infrastructure [25]. Extending neutrino monitoring to large, deep geological repositories remains a distant prospect given the impractical detector masses, background suppression, and lifetimes required [24].

*Acknowledgments*—We thank the company *Electricité de France* (EDF); the European fund FEDER; the Région de Champagne-Ardenne; the Département des Ardennes; and the Communauté de Communes Ardenne Rives de Meuse. We acknowledge the support of the CEA, CNRS and IN2P3, the computer center CC-IN2P3, and LabEx UnivEarthS in France; the Max Planck Gesellschaft, the Deutsche Forschungsgemeinschaft DFG, the Transregional Collaborative Research Center TR27, the excellence cluster "Origin and Structure of the Universe," and the Maier-Leibnitz-Laboratorium Garching in Germany; the Ministry of Education, Culture, Sports, Science and Technology of Japan (MEXT), and the Japan Society for the Promotion of Science (JSPS); the Ministerio de Economía, Industria y Competitividad in Spain; the Department of Energy and the National Science Foundation in the United States; the Russian Academy of Sciences, the Kurchatov Institute, and the Russian Foundation for Basic Research (RFBR); the Brazilian Ministry of Science, Technology and Innovation (MCTI), the Financiadora de Estudos e Projetos (FINEP), the Conselho Nacional de Desenvolvimento Científico e Tecnológico (CNPq), the São Paulo Research Foundation (FAPESP), and the Brazilian Network for High Energy Physics (RENAFAE).

*Data availability*—The data that support the findings of this article are not publicly available. The data are available from the authors upon reasonable request.

[1] C. L. Cowan, F. Reines, F. B. Harrison, H. W. Kruse, and A. D. McGuire, Science **124**, 103 (1956).
[2] J. Dos Anjos *et al.*, IAEA Report No. STR-361, 2008.
[3] A. Borovoi and L. Mikaelyan, Sov. At. Energy **44**, 589 (1978).
[4] A. I. Afonin, A. A. Borovoi, Y. L. Dobrynin, S. N. Ketov, V. I. Kopeikin, L. A. Mikaelyan, M. D. Skorokhvatov, S. V. Tolokonnikov, and A. N. Kheruvimov, JETP Lett. **41**, 435 (1985), https://inspirehep.net/literature/222363.
[5] A. Bernstein, G. Baldwin, B. Boyer, M. Goodman, J. Learned, J. Lund, D. Reyna, and R. Svoboda, Sci. Global Secur. **18**, 127 (2010).
[6] C. Stewart, A. Abou-Jaoude, and A. Erickson, Nat. Commun. **10**, 3527 (2019).
[7] Double Chooz Collaboration, Nat. Phys. **16**, 558 (2020).
[8] F. Ardellier *et al.* (Double Chooz Collaboration), arXiv:hep-ex/0606025.
[9] H. de Kerret *et al.* (Double Chooz Collaboration), Eur. Phys. J. C **82**, 804 (2022).
[10] F. P. An *et al.* (Daya Bay Collaboration), Phys. Rev. Lett. **133**, 151801 (2024).
[11] S. G. Yoon *et al.* (RENO Collaboration), Phys. Rev. D **104**, L111301 (2021).
[12] T. Abrahão *et al.* (Double Chooz Collaboration), J. High Energy Phys. 01 (2021) 190.
[13] Y. Abe *et al.* (Double Chooz Collaboration), Phys. Rev. D **87**, 011102 (2013).
[14] Y. Abe *et al.* (Double Chooz Collaboration), J. High Energy Phys. 01 (2016) 163.
[15] V. I. Kopeikin, L. A. Mikaelyan, and V. V. Sinev, Phys. At. Nucl. **64**, 849 (2001).
[16] V. I. Kopeikin, Phys. At. Nucl. **75**, 143 (2012).
[17] R. Sanchez, J. Mondot, Žarko Stankovski, A. Cossic, and I. Zmijarevic, Nucl. Sci. Eng. **100**, 352 (1988).
[18] T. A. *et al.*, J. Nucl. Sci. Technol. **37**, 845 (2000).
[19] A. Santamarina *et al.*, OECD 2009 NEA No. 6807, ISBN 978-92-64-99074-6 (2009).

[20] L. Périssé, A. Onillon, X. Mougeot, M. Vivier, T. Lasserre, A. Letourneau, D. Lhuillier, and G. Mention, Phys. Rev. C **108**, 055501 (2023).
[21] P. Vogel and J. F. Beacom, Phys. Rev. D **60**, 053003 (1999).
[22] M. Tanabashi *et al.* (Particle Data Group), Phys. Rev. D **98**, 030001 (2018).
[23] See End Matter for additional information on the time evolution of the residual antineutrino signal from reactor cores and spent-fuel pools.
[24] O. Akindele *et al.*, 10.2172/1826602 (2021).
[25] V. Brdar, P. Huber, and J. Kopp, Phys. Rev. Appl. **8**, 054050 (2017).

## End Matter

The residual antineutrino signal measured in the two detectors is the time-integrated sum of several distinct contributions, arising from fuel remaining in the shutdown reactor cores and from spent-fuel stored in the two spent-fuel pools. As discussed in the main text, these components exhibit different temporal evolutions: the in-core contribution decreases rapidly after shutdown, while the spent-fuel pool contribution is longer-lived and can show discrete changes when a new batch of discharged fuel is transferred to a storage pool. This behavior is illustrated in Figs. 6 and 7 for the near detector. In the main text, we reported the uncertainty on the total predicted number of events integrated over the four reactor-off periods. For each individual period, a mild time dependence of this uncertainty is expected due to the evolving isotopic composition of the irradiated fuel after shutdown. For the purpose of these two plots, we adopt the average uncertainties as a first-order approximation, which is sufficient at the current level of precision.

Figure 6 shows the long-term buildup and decay of the predicted residual antineutrino contribution from the spent-fuel pools to the near detector. Each discharged fuel batch contributes a time-dependent component that decreases as the fuel cools. Because the pool signal is the superposition of contributions from fuel discharged over several successive reactor cycles, it does not follow a simple monotonic decay. Instead, the total contribution evolves in a quasi-periodic sawtooth pattern: the rate decreases between refueling periods, then increases again when a new batch of recently irradiated assemblies is added to the pool. After

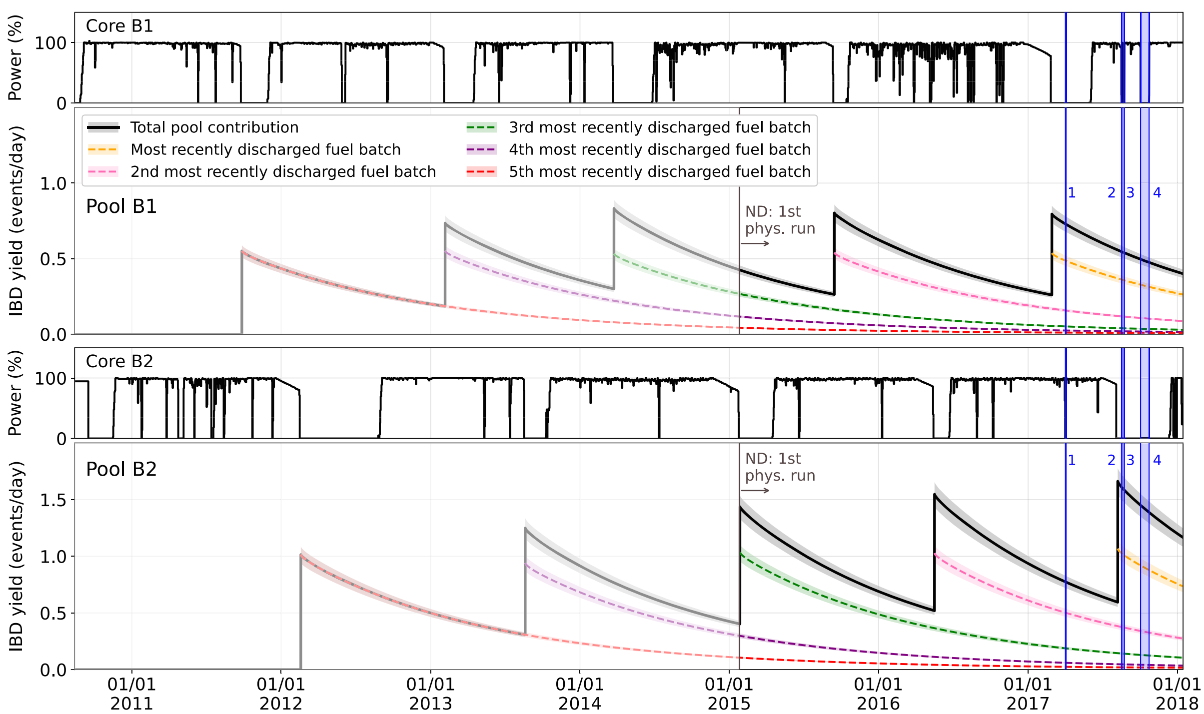


FIG. 6. Predicted IBD yield in the near detector from spent-fuel assemblies stored in the B1 pool (top) and B2 pool (bottom), with the thermal power of the corresponding reactor core shown in the upper panels. Colored curves show the contributions from fuel batches discharged after successive reactor irradiation cycles, while the black curve represents the total pool contribution. The shaded bands represent the corresponding $1\sigma$ uncertainties as described in the text. For this calculation, transfer of the discharged assemblies to the pool is considered to occur three days after reactor shutdown. The vertical blue bands mark the four 2017 reactor-off periods used in this analysis. Assemblies discharged before 2012 were not included in the simulation, as they had already been removed from the spent-fuel pools for reprocessing. The larger contribution from the B2 pool is mainly due to its shorter distance to the detector.

several cycles, the repeated addition of fresh spent fuel and the fading of older contributions lead to a quasiequilibrium regime. This behavior illustrates the strong dependence of the pool signal on the detailed irradiation, discharge, and storage history of the site. At any given time, the pool signal is typically dominated by the most recently discharged batch, with successively smaller contributions from older batches as their residual activity decreases with cooling time. We found that averaged over B1 and B2 pools, for the last three reactor-off periods, about 64%, 23%, 9%, 3%, and 1% of the spent-fuel pool signal arise from the fifth most recently discharged batches.

Figure 7 shows the predicted time evolution of the residual IBD yield in the near detector during each of the four reactor-off periods used in this analysis. In all cases, the contribution from fuel remaining in the recently shutdown core dominates and decreases rapidly with time, reflecting the decay of short-lived fission products accumulated during the preceding irradiation cycle. By contrast, the contributions from spent fuel stored in the B1 and B2 spent-fuel pools evolve only weakly over the duration of a given period, as they are governed by longer-lived isotopes and by the cumulative inventory of assemblies discharged over several previous cycles. As a result, the total residual signal exhibits a fast initial drop when the in-core component is large, followed by a slower evolution in which the pool contribution becomes increasingly important. The figure further illustrates that the relative weights of the in-core and spent-fuel pool components depend on the specific shutdown and refueling configuration of each period, with the longest fourth period being the most sensitive to the long-lived pool contribution. After the initial rapid decrease following shutdown, the predicted residual signal in the near detector is typically of order 3.5–4 events/day during the reactor-off periods. Of these, about 1.5–2 events/day arise from the spent-fuel pools, compared with about 900 events/day from the cores at full reactor power.

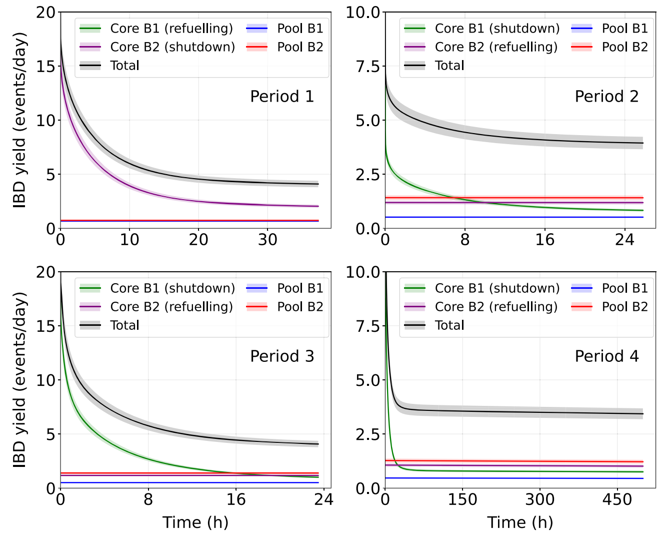


FIG. 7. Predicted IBD yield in the near detector for each reactor-off period. The contribution from in-core and spent-fuel pools are shown as well as the total contribution. The shaded bands represent the corresponding $1\sigma$ uncertainties as described in the text. The differences observed between periods reflect the specific shutdown and refuelling configuration, the irradiation history of the fuel at the time of shutdown, and the different distances between each source and the detector. In this analysis, only physics runs starting at least 30 min after the beginning of each reactor-off period were included. This excludes the early phase of rapid signal decrease due to short-lived fission products. With this selection, uncertainties in the reactor-off start time have a negligible impact.